Experimental Validation of the OFDM Bit Error Probability for a Moving Receive Antenna

Ronald Nissel, Martin Lerch and Markus Rupp
Institute of Telecommunications, Vienna University of Technology, Vienna, Austria
Email: {rnissel, mlerch, mrupp}@nt.tuwien.ac.at

***Abstract*—For an orthogonal frequency-division multiplexing system with pilot-symbol aided channel estimation, we compare the measured bit error ratio to the theoretical bit error probability. In order to measure mobile physical systems, we utilize the Vienna Wireless Testbed which has been augmented by a rotation wheel unit. The analytical solution assumes Rayleigh fading, additive Gaussian noise, and an arbitrary linear interpolation method to estimate the unknown channel taps. Our measurements confirm our assumptions and demonstrate convincingly that our theoretical expressions accurately model the true physical behavior, even for speeds of up to 100 km/h.**

I. Introduction

Nowadays, most wireless communication standards (DAB, LTE, WIFI 802.11) employ Orthogonal Frequency Division Multiplexing (OFDM) as their modulation technique. While we have a good knowledge of what to expect in coherent transmissions over wireless channels in idealistic setups, the implications of practical systems are by far not so well understood. In particular high speed scenarios as they appear in car/train to infrastructure communications by LTE require a solid understanding of the transmission chain. Coherent transmission requires channel knowledge which typically comes by estimation based on training or so-called pilot symbols, i.e., known symbols at transmitter and receiver side. Pilot-symbol-Aided Channel Estimation (PACE) is usually considered in this context whereby the channel at data positions is estimated by interpolation. The optimal linear interpolation in terms of Minimum Mean Squared Error (MMSE) was derived in [1]. However, an MMSE solution requires a-priori knowledge of the channel statistics and a matrix inversion. This motivated other authors to investigate different interpolation methods e.g., spline [2], 2D Deslauriers-Dubuc [3] and 2D low-pass [4]. As a comparison measure the Bit Error Ratio (BER) was obtained through Monte Carlo simulations. Such simulations require a long simulation time and do not offer analytical insights. This recently motivated us to derive an analytical Bit Error Probability (BEP) expression for arbitrary linear interpolation methods [5] which can, for example, be used to find an improved pilot pattern design or to determine the optimal trade-off between pilot and data symbol power [6].

Mobile wireless communication channels are characterized by time-varying multipath propagation [7], i.e., due to multiple scatterers, the electromagnetic signal can propagate along several different paths which causes frequency-selectivity and time-selectivity. The first can be combated by inserting a cyclic prefix while the latter leads to Inter-Carrier Interference (ICI) and can only be combated by sophisticated and costly signal processing algorithms [8].

Although theoretical expressions and simulations are very useful, they represent only a simplified abstraction and eventually, only the performance in real world scenarios matters. However, testing new ideas (e.g., interpolation methods) in real world scenarios is too costly. Therefore testbeds are employed. They are regarded as a test vehicle between simulations and real world scenarios and often reveal practical problems which have not been considered so far.

Testbeds which support mobile receivers typically place the measurement equipment in a car [9]–[11]. The achievable velocity of such measurement setup is very limited. To emulate higher velocities, [12] proposed the usage of a smaller subcarrier spacing and claimed that this is equivalent to higher velocities. The drawback of this method is a reduction of the bandwidth and therefore loss of frequency-selectivity. Nonetheless, such car measurements lack repeatability and controllability, which constitutes the main problem for a fair comparison of different transmission techniques.

Our approach for repeatable and fully controllable measurements at high-velocities is based on the rotation of a receive antenna around a central pivot [13]. Because of a short transmission time, the effective rotation angle is very small so that the antenna movement resembles a linear translation.

The measurement parameters are chosen similar to the LTE standard which was designed for high velocities [14]. Very often in the OFDM literature, time-selective channels are modeled so that ICI becomes a major impediment. Assuming a carrier frequency of 2.5 GHz and a Jakes Doppler spectrum, a velocity of 100 km/h corresponds to a Signal-to-Interference Ratio (SIR) of 35 dB [15] so that the ICI part can usually be neglected, as we observe in our measurements. Note that phase noise, frequency offsets and non-linear amplifier also lead to ICI. However, because of our high-quality hardware this does not constitute an issue.

Novel contribution

1) We present a method for repeatable and controllable high-speed measurements and show the validity of commonly made assumptions (Rayleigh fading, Gaussian noise) for our measurement setup.

2) We show the excellent agreement between our derived theoretical BEP expressions and the measured BER results.

3) We show experimentally that in our setup, even speeds of 100 km/h do not cause significant ICI.

978-1-4799-4449-1/14/$31.00 ©2014 IEEE

$$\Pr\left(\Re\left\{\frac{y_{l,k}}{\hat{h}_{l,k}}\right\}<\frac{a}{\sqrt{b}}\middle|\frac{q_r+\mathrm{j}q_i}{\sqrt{b}}\right)=\frac{1}{2}-\frac{1}{2}\Big[q_r\Re\{\alpha_{l,k}\}-q_i\Im\{\alpha_{l,k}\}-a\beta_{l,k}\Big]\times$$
$$\times\left[\big[(q_r^2+q_i^2)P_{\mathrm{S}_{l,k}}+bP_{\mathrm{ICI+noise}_{l,k}}-2a\left(q_r\Re\{\alpha_{l,k}\}-q_i\Im\{\alpha_{l,k}\}\right)+a^2\beta_{l,k}\big]\beta_{l,k}-\left(q_i\Re\{\alpha_{l,k}\}+q_r\Im\{\alpha_{l,k}\}\right)^2\right]^{-\frac{1}{2}} \tag{1}$$

II. System Model

In our OFDM model, $x_{l,k}\in\mathbb{C}$ denotes the transmitted, unit power, data symbols at subcarrier-position l ($l=1,2\ldots,L$) and time-position k ($k=1,2\ldots,K$), chosen from a Gray coded 4-Quadrature Amplitude Modulation (QAM) respectively 16-QAM signal constellation. The received data symbol $y_{l,k}\in\mathbb{C}$ depends on the transmitted data symbol as follows:

$$y_{l,k}=h_{l,k}x_{l,k}+z_{l,k}, \tag{2}$$

where $h_{l,k}\in\mathbb{C}$ denotes the Rayleigh fading channel with signal power $P_{\mathrm{S}_{l,k}}=\mathbb{E}\{h_{l,k}h_{l,k}^*\}$ and $z_{l,k}\sim\mathcal{CN}(0,P_{\mathrm{ICI+noise}_{l,k}})$ the white additive Gaussian noise, which includes also ICI.

Dividing Equation (2) by the estimated channel $\hat{h}_{l,k}$ leads to the zero forcing equalization and delivers a Least Squares (LS) estimate of the transmitted data symbol $x_{l,k}$:

$$\hat{x}_{l,k}=\frac{y_{l,k}}{\hat{h}_{l,k}}. \tag{3}$$

For perfect channel knowledge ($\hat{h}_{l,k}=h_{l,k}$), the zero forcing equalizer corresponds to the Maximum Likelihood (ML) detection. However, for PACE such equalization is no longer optimal in the ML sense [16], but due to its simplicity still a reasonable choice.

The required channel estimate in (3) is found by interpolation (weighted average) of known LS estimates at pilot positions:

$$\hat{h}_{l,k}=\sum_{\{l_p,k_p\}\in\mathcal{P}}\left(\mathbf{w}_{l,k}^*\right)_{\{l_p,k_p\}}\frac{y_{l_p,k_p}}{x_{l_p,k_p}}. \tag{4}$$

Set $\mathcal{P}$ is a collection of the two-dimensional (2D) pilot position indexes whereas the number of pilot symbols is given by its cardinality $|\mathcal{P}|$. Rewriting Equation (4) in vector notation leads to:

$$\hat{h}_{l,k}=\mathbf{w}_{l,k}^H\hat{\mathbf{h}}_{\mathcal{P}}^{\mathrm{LS}}, \tag{5}$$

where the vector $\hat{\mathbf{h}}_{\mathcal{P}}^{\mathrm{LS}}\in\mathbb{C}^{|\mathcal{P}|\times 1}$ consists of the vectorized LS estimates at pilot positions and the vector function $\mathbf{w}_{l,k}\in\mathbb{C}^{|\mathcal{P}|\times 1}$ depends on the interpolation method (e.g., MMSE, linear, spline). We also assume that each pilot symbol has unit power.

III. Bit Error Probability for Pilot-Symbol-Aided Channel Estimation

We recently derived a closed-form expression for the BEP of an OFDM system that utilizes PACE [5]. The BEP for 16-QAM is given as:

$$\begin{aligned}\mathrm{BEP}_{l,k}^{16\mathrm{QAM}}(\mathbf{w}_{l,k})=&\\ &\frac{1}{16}\sum_{\substack{q_r\in\\ \{1,3\}}}\sum_{\substack{q_i\in\{-3,\\ -1,1,3\}}}\Pr\left(\Re\left\{\frac{y_{l,k}}{\hat{h}_{l,k}}\right\}<0\middle|\frac{q_r+\mathrm{j}q_i}{\sqrt{10}}\right)+\\ &\frac{1}{16}\sum_{\substack{q_i\in\{-3,\\ -1,1,3\}}}\left(1-\Pr\left(\frac{-2}{\sqrt{10}}<\Re\left\{\frac{y_{l,k}}{\hat{h}_{l,k}}\right\}<\frac{2}{\sqrt{10}}\middle|\frac{1+\mathrm{j}q_i}{\sqrt{10}}\right)\right)\\ &+\frac{1}{16}\sum_{\substack{q_i\in\{-3,\\ -1,1,3\}}}\Pr\left(\frac{-2}{\sqrt{10}}<\Re\left\{\frac{y_{l,k}}{\hat{h}_{l,k}}\right\}<\frac{2}{\sqrt{10}}\middle|\frac{3+\mathrm{j}q_i}{\sqrt{10}}\right),\end{aligned} \tag{6}$$

and for 4-QAM by:

$$\begin{aligned}\mathrm{BEP}_{l,k}^{4\mathrm{QAM}}(\mathbf{w}_{l,k})=&\frac{1}{2}\Pr\left(\Re\left\{\frac{y_{l,k}}{\hat{h}_{l,k}}\right\}<0\middle|\frac{1+\mathrm{j}}{\sqrt{2}}\right)\\ &+\frac{1}{2}\Pr\left(\Re\left\{\frac{y_{l,k}}{\hat{h}_{l,k}}\right\}<0\middle|\frac{1-\mathrm{j}}{\sqrt{2}}\right).\end{aligned} \tag{7}$$

For a compact description of the probabilities $\Pr(\cdot)$, we define two new variables, $\alpha_{l,k}\in\mathbb{C}$ and $\beta_{l,k}\in\mathbb{R}$:

$$\alpha_{l,k}=\mathbf{r}_{\hat{\mathbf{h}}_{\mathcal{P}}^{\mathrm{LS}},h_{l,k}}^H\mathbf{w}_{l,k} \tag{8}$$

$$\beta_{l,k}=\mathbf{w}_{l,k}^H\mathbf{R}_{\hat{\mathbf{h}}_{\mathcal{P}}^{\mathrm{LS}}}\mathbf{w}_{l,k}, \tag{9}$$

whereas $\mathbf{r}_{\hat{\mathbf{h}}_{\mathcal{P}}^{\mathrm{LS}},h_{l,k}}=\mathbb{E}\{\hat{\mathbf{h}}_{\mathcal{P}}^{\mathrm{LS}}h_{l,k}^*\}\in\mathbb{C}^{|\mathcal{P}|\times 1}$ denotes the cross-correlation vector and $\mathbf{R}_{\hat{\mathbf{h}}_{\mathcal{P}}^{\mathrm{LS}}}=\mathbb{E}\{\hat{\mathbf{h}}_{\mathcal{P}}^{\mathrm{LS}}(\hat{\mathbf{h}}_{\mathcal{P}}^{\mathrm{LS}})^H\}\in\mathbb{C}^{|\mathcal{P}|\times|\mathcal{P}|}$ the autocorrelation matrix. The required probability is then given by Equation (1) which is applied in (6) and (7) to calculate the BEP at subcarrier-position l and time-position k.

IV. Vienna Wireless Testbed

Our measurements are based on the Vienna Wireless Testbed that has been augmented by a rotating wheel unit to generate high speed movements. The concept for repeatable and controllable high speed measurements was already proposed in [13] but it took us three additional years to finish the setup. The basic idea is to rotate the receive antenna around a central pivot. Compared to a linear guide we avoid the repeated acceleration and deceleration step, so that high velocities can be achieved. Our setup represents a scenario in which the rotational speed is low relative to the transmission time, so that the antenna moves approximately linear during the transmission. Assume for example a velocity of 100 km/h (4.4 revolutions per second

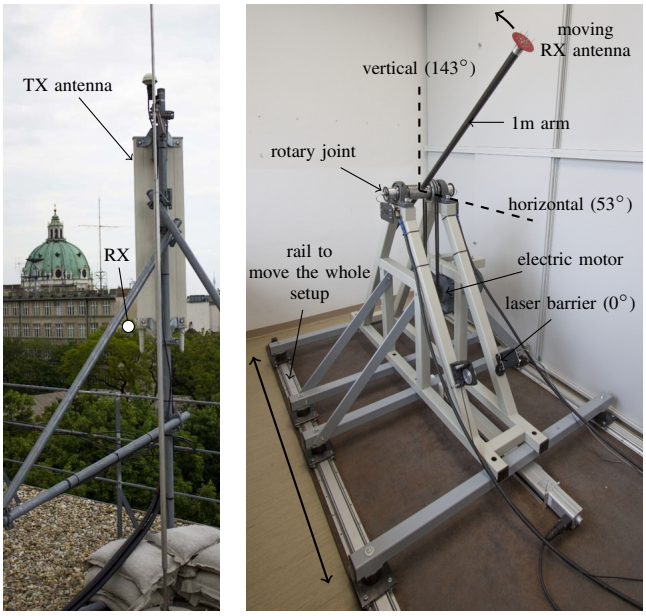

Fig. 1. Vienna Wireless Testbed: transmit antenna, located on the rooftop (above the 5th floor) and moving receive antenna, located indoor on the 5th floor of the opposite building.

for a 1 m arm). Then, for a transmission time of 1 ms, the antenna moves only by $4.4\,\mathrm{rps} \times 1\,\mathrm{ms} \times 360^\circ = 1.6^\circ$ which is close enough to a linear movement. Additionally, the whole rotation unit is portable so that it can be placed e.g., next to a rail track.

The Vienna Wireless Testbed performs quasi real-time measurements, i.e., the signal is generated off-line, transmitted over a wireless channel in real-time and then again evaluated off-line [17]. Its main parts are:

- The 16-bit digital-to-analog and analog-to-digital converter, connected to a personal computer and operating at a sampling frequency of $f_\mathrm{s} = 200\,\mathrm{MHz}$.
- The radio frequency front end which up-converts the signal to 2.5 GHz (respectively down-converts). The front end is designed for an intermediate frequency of $f_\mathrm{IF} = 70\,\mathrm{MHz}$ so that the signal has to be digitally up-converted respectively down-converted.
- The transmit antenna, located on the rooftop of our university (see Figure 1a) and the moving (rotates around a central pivot) receive antenna, mounted on a rotation wheel unit (see Figure 1b) which is placed on a rail so that it can be moved within a range of 0.82 m.
- A Global Positioning System (GPS) module and a rubidium frequency standard for synchronization of transmitter and receiver.
- The laser barrier together with a trigger system which determine the starting time instance of the transmission at a specific antenna position. The laser barrier defines the 0° reference point.

TABLE I
MEASUREMENT PARAMETERS

Modulation order	4-QAM and 16-QAM
Number of subcarriers, L	145
Number of OFDM symbols, K	49
Pilot pattern	rectangular
Frequency pilot spacing	6
Time pilot spacing	4
Carrier frequency	2.507 GHz
Subcarrier spacing, Δf	15 kHz
CP duration, T_CP	4.67 μs
Velocity	50 km/h and 100 km/h
Angle position range	32°...72°
Rail position range	0.05 ...0.75 m
Number of random positions, I	1200
Number of attenuation levels, A	8, in 5 dB steps

V. MEASUREMENT METHODOLOGY

The proper sampled (f_s) and digitally up-converted (f_IF) OFDM signal in the time domain (without cyclic prefix) is generated by an inverse fast Fourier transform:

$$\mathbf{s}_k^T = \mathrm{IFFT}\Big\{ \begin{bmatrix} \mathbf{0}_1^T & x_{1,k} & \cdots & x_{L,k} & \mathbf{0}_2^T & x_{L,k}^* & \cdots & x_{1,k}^* & \mathbf{0}_3^T \end{bmatrix} \Big\}, \tag{10}$$

where $\mathbf{0}_1$, $\mathbf{0}_2$ and $\mathbf{0}_3$ are zero vectors of size $\left\lceil \frac{f_\mathrm{IF}}{\Delta f} - \frac{L}{2} \right\rceil$, $\left\lfloor \frac{f_\mathrm{s} - 2f_\mathrm{IF}}{\Delta f} - L \right\rfloor$ and $\left\lfloor \frac{f_\mathrm{IF}}{\Delta f} - \frac{L}{2} \right\rfloor$ (Δf denotes the subcarrier spacing). The OFDM signal vector $\mathbf{s}_k \in \mathbb{R}^{\lfloor f_\mathrm{s}/\Delta f \rfloor \times 1}$ together with the cyclic prefix, i.e., copying the last $\lfloor f_\mathrm{s} T_\mathrm{CP} \rfloor$ samples and placing it in front, provides immediately the input samples for the digital-to-analog converter which are transmitted over a real-world channel.

The received data symbols $y_{l,k}$ are obtained similar to the signal generation, but in reverse order, i.e., removing the cyclic prefix, fast Fourier transform, and then choosing the appropriate elements in the frequency domain.

Thus, the whole measurement setup can be viewed as a black box where $x_{l,k}$ represents the input and $y_{l,k}$ its output. However, one must always keep in mind the limitations imposed by real-world hardware and in particular the saturation of power amplifiers.

For each transmission, $K+2$ OFDM symbols are sent over the wireless channel whereas each OFDM symbol consists of $L+2$ subcarriers. To estimate the noise power at the receiver, the first and last OFDM symbols are set to zero ($x_{l,0} = 0$, $x_{l,K+1} = 0$). Similar, the ICI-plus-noise power $\hat{P}_\mathrm{ICI+noise}^{\{a\}}$ is estimated by setting the first and last subcarriers to zero ($x_{0,k} = 0$, $x_{L+1,k} = 0$). For our chosen parameters, measurements have shown that the ICI power can be neglected compared to the noise power: at highest velocity (100 km/h) and highest transmit power (Signal-to-Interference plus Noise Ratio (SINR) of 31 dB), the ICI power is 5.5 dB lower than the noise power. For lower velocities and lower transmit powers this gap further increases.

Each measurement realization $\{i, a\}$ corresponds to a specific:

- position-index i ($i = 1, 2 \ldots, I$), composed of rail-position and angle-position
- attenuation-index a ($a = 0, 1 \ldots, A$) which corresponds to a specific attenuation in the radio frequency front end of the transmitter. The transmission at lowest attenuation ($a = 0$) is solely used for the estimation of the second-order statistics, and not to transmit data.

At an angle-position of 143°, the antenna rotates in the same direction as the rotation unit moves on the rail, so that the number of independent measurement realizations is reduced. Additionally, the average received power as well as the correlation matrices depend strongly on the angle-position. Exploiting the whole 360° range is therefore not feasible with respect to our analytical assumptions, so that only an angle-range of 32°...72° is assessed. Furthermore, for each transmission, we use randomly one out of four transmit antennas, supported by the testbed, in order to obtain more independent measurement realizations whereas pre-equalization guarantees constant average receive power for different antennas.

Because the absolute value of the received symbols has no influence, we normalize them to have a mean signal power of one, so that the channel correlation matrices are independent of the transmit power.

By applying the measured LS channel estimates:

$$\hat{h}_{l,k}^{\mathrm{LS},\{i,a\}} = \frac{y_{l,k}^{\{i,a\}}}{x_{l,k}^{\{i,a\}}}, \tag{11}$$

we estimate the signal power by:

$$\hat{P}_{\mathrm{S}_{l,k}} = \frac{1}{I} \sum_{i=1}^{I} \left| \hat{h}_{l,k}^{\mathrm{LS},\{i,0\}} \right|^2 - \kappa \hat{P}_{\mathrm{ICI+noise}}^{\{0\}}, \tag{12}$$

where $a = 0$ indicates the transmission at highest SINR and κ corrects the error caused by the LS estimation at higher modulation orders (division by $x_{l,k}$). Note that the signal power depends on subcarrier-position and time-position in order to be consistent with the estimated cross-correlation vector $\mathbf{r}_{\hat{\mathbf{h}}_{\mathcal{P}}^{\mathrm{LS}}, h_{l,k}}$ and the estimated correlation matrix $\mathbf{R}_{\hat{\mathbf{h}}_{\mathcal{P}}^{\mathrm{LS}}}$, both given by:

$$\hat{\mathbf{r}}_{\hat{\mathbf{h}}_{\mathcal{P}}^{\mathrm{LS}}, h_{l,k}} = \frac{1}{I} \sum_{i=1}^{I} \hat{\mathbf{h}}_{\mathcal{P}}^{\mathrm{LS},\{i,0\}} \left(\hat{h}_{l,k}^{\mathrm{LS},\{i,0\}} \right)^* \tag{13}$$

$$\hat{\mathbf{R}}_{\hat{\mathbf{h}}_{\mathcal{P}}^{\mathrm{LS}}}^{\{a\}} = \hat{\mathbf{R}}_{\mathbf{h}_{\mathcal{P}}} + \hat{P}_{\mathrm{ICI+noise}}^{\{a\}} \mathbf{I}_{|\mathcal{P}|}, \tag{14}$$

whereas Equation (13) is valid only at data position. The identity matrix $\mathbf{I}_{|\mathcal{P}|}$ has size $|\mathcal{P}|$ and the channel autocorrelation matrix $\hat{\mathbf{R}}_{\mathbf{h}_{\mathcal{P}}}$ is estimated by:

$$\hat{\mathbf{R}}_{\mathbf{h}_{\mathcal{P}}} = \frac{1}{I} \sum_{i=1}^{I} \hat{\mathbf{h}}_{\mathcal{P}}^{\mathrm{LS},\{i,0\}} \left(\hat{\mathbf{h}}_{\mathcal{P}}^{\mathrm{LS},\{i,0\}} \right)^H - \hat{P}_{\mathrm{ICI+noise}}^{\{0\}} \mathbf{I}_{|\mathcal{P}|}. \tag{15}$$

Furthermore, we define the estimated SINR as follows:

$$\mathrm{SINR}^{\{a\}} = \frac{\frac{1}{KL} \sum_{l=1}^{L} \sum_{k=1}^{K} \hat{P}_{\mathrm{S}_{l,k}}}{\hat{P}_{\mathrm{ICI+noise}}^{\{a\}}} = \frac{1}{\hat{P}_{\mathrm{ICI+noise}}^{\{a\}}}. \tag{16}$$

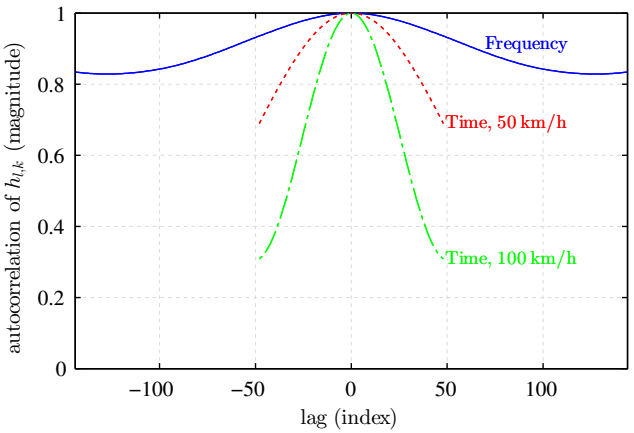

Fig. 2. Measured autocorrelation function of the channel, dependent of either subcarrier-position (1 unit = 15 kHz) or time-position (14 unit = 1 ms) lag.

The next section shows the measurement results for which we consequently distinguish between:

A. Analytical Bit Error Probability

The estimated second order statistics $\hat{P}_{\mathrm{S}_{l,k}}$, $\hat{P}_{\mathrm{ICI+noise}}^{\{a\}}$, $\hat{\mathbf{R}}_{\hat{\mathbf{h}}_{\mathcal{P}}^{\mathrm{LS}}}^{\{a\}}$, and $\hat{\mathbf{r}}_{\hat{\mathbf{h}}_{\mathcal{P}}^{\mathrm{LS}}, h_{l,k}}$ are substituted in Equation (1) to calculate the probabilities $\Pr(\cdot)$ which in turn are inserted in Equation (6) and (7) to calculate the analytical BEP as a function of SINR (corresponds to a). Additionally, this result is averaged over all (data) subcarrier- and time-positions.

B. Measured Bit Error Ratio

Equalization of the received symbol $y_{l,k}^{\{i,a\}}$ (Equation (3)) delivers an estimate of the transmitted data symbol and, after demapping (minimal Euclidean distances, Gray coding), a possible bit error. Averaging this result over all (data) subcarrier, time, and measurement-positions then gives the measured BER as a function of SINR.

VI. Measurement Results

Table I summarizes our chosen measurement parameters. The assumptions of Rayleigh fading and Gaussian noise are supported by a Lilliefors [18] test (5% significance), performed at each subcarrier-position and time-position. In only 5.5% of the cases the null hypothesis of Gaussian noise was rejected, while the assumption of Rayleigh fading (real part and imaginary part are Gaussian distributed) was rejected in 6.9% of the cases. Figure 2 shows the measured autocorrelation functions under the assumption of wide sense stationarity, uncorrelated scatterers and a separable time-frequency correlation function.

For the comparison of the BER with the BEP, we consider three specific interpolation methods: a 2D MMSE estimation [1] $\mathbf{w}_{l,k}^{\mathrm{MMSE}} = \mathbf{R}_{\hat{\mathbf{h}}_{\mathcal{P}}^{\mathrm{LS}}}^{-1} \mathbf{r}_{\hat{\mathbf{h}}_{\mathcal{P}}^{\mathrm{LS}}, h_{l,k}}$, a linear- and a spline-interpolation. The latter two are obtained by utilizing the MATLAB build-in 1D interpolation functions first in one dimension, and then again in the other dimension. Figures 3a and 3b show the result for 50 km/h respectively 100 km/h

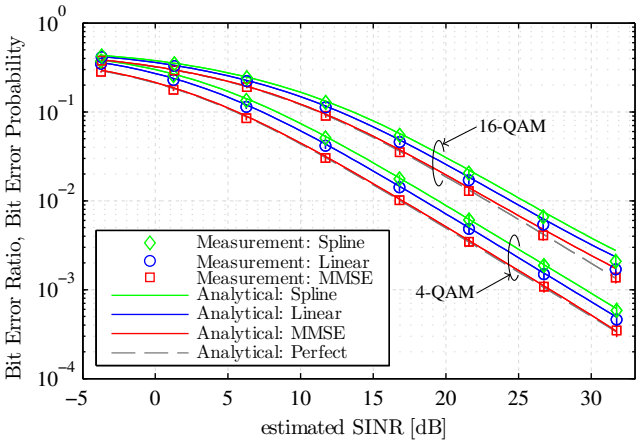

(a) For 50 km/h.

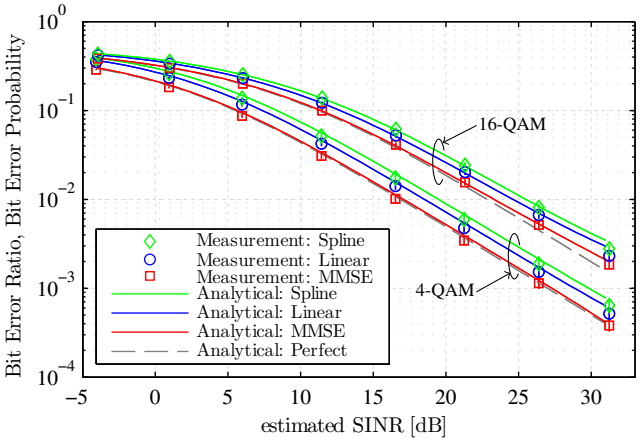

(b) For 100 km/h.

Fig. 3. BER vs. BEP as a function of SINR, influence of interpolation, measurements confirm analytical predictions.

where it is visible that the theoretical BEP and the measured BER coincide. Due to a highly correlated channel, we can identify three effects: first, the MMSE interpolation performs close to perfect channel knowledge, second, the BER does not depend on the velocity since the ICI power is smaller than the noise power, and third, spline interpolation performs worse because it uses first and second derivatives which lead to high errors if the noise is larger than variations caused by the channel.

VII. Conclusion

We showed that the BEP expression for pilot-symbol-aided channel estimation, utilizing arbitrary linear interpolation methods, can be applied in real-world channels. The assumptions of Rayleigh fading and Gaussian noise are appropriate for our chosen measurement setup. Furthermore, our results serve as a good starting point for high speed measurements of enhanced signal processing algorithms, such as ICI mitigation techniques (by increasing the velocity or decreasing the subcarrier spacing) or filter bank multicarrier transmissions.

Acknowledgment

This work has been funded by the Christian Doppler Laboratory for Wireless Technologies for Sustainable Mobility, the A1 Telekom Austria AG, and the KATHREIN-Werke KG. The financial support by the Federal Ministry of Economy, Family and Youth and the National Foundation for Research, Technology and Development is gratefully acknowledged.

References

[1] P. Hoeher, S. Kaiser, and P. Robertson, "Two-dimensional pilot-symbol-aided channel estimation by Wiener filtering," *IEEE International Conference on Acoustics, Speech, and Signal Processing (ICASSP'97)*, vol. 3, pp. 1845–1848, 1997.

[2] M.-H. Hsieh and C.-H. Wei, "Channel estimation for OFDM systems based on comb-type pilot arrangement in frequency selective fading channels," *IEEE Transactions on Consumer Electronics*, vol. 44, no. 1, pp. 217–225, 1998.

[3] X. Dong, W.-S. Lu, and A. Soong, "Linear interpolation in pilot symbol assisted channel estimation for OFDM," *IEEE Transactions on Wireless Communications*, vol. 6, no. 5, pp. 1910–1920, 2007.

[4] M. Yalcin and A. Akan, "Doubly-selective channel estimation for OFDM systems," in *IEEE 9th Malaysia International Conference on Communications (MICC)*, Dec. 2009, pp. 6–10.

[5] R. Nissel, M. Lerch, M. Šimko, and M. Rupp, "Bit error probability for pilot-symbol-aided OFDM channel estimation in doubly-selective channels," in *18th International ITG Workshop on Smart Antennas (WSA 2014)*, Erlangen, Germany, Mar. 2014.

[6] M. Šimko, Q. Wang, and M. Rupp, "Optimal pilot symbol power allocation under time-variant channels," *EURASIP Journal on Wireless Communications and Networking*, vol. 2012, no. 1, pp. 1–11, 2012.

[7] F. Hlawatsch and G. Matz, *Wireless Communications over Rapidly Time-Varying Channels*. Amsterdam: Academic Press, 2011.

[8] F. Pena-Campos, R. Carrasco-Alvarez, O. Longoria-Gandara, and R. Parra-Michel, "Estimation of fast time-varying channels in OFDM systems using two-dimensional prolate," *IEEE Transactions on Wireless Communications*, vol. 12, no. 2, pp. 898–907, Feb. 2013.

[9] N. Miyazaki, S. Nanba, and S. Konishi, "MIMO-OFDM throughput performances on MIMO antenna configurations using LTE-based testbed with 100 mhz bandwidth," in *2010 IEEE 72nd Vehicular Technology Conference Fall (VTC 2010-Fall)*, Sept. 2010, pp. 1–5.

[10] P. Mahasukhon, H. Sharif, M. Hempel, T. Zhou, and T. Ma, "Distance and throughput measurements in mobile WiMAX test bed," in *IEEE MILITARY COMMUNICATIONS CONFERENCE, 2010-MILCOM*, 2010, pp. 154–159.

[11] K. Jang, M. Han, S. Cho, H.-K. Ryu, J. Lee, Y. Lee, and S. B. Moon, "3G and 3.5 G wireless network performance measured from moving cars and high-speed trains," in *Proceedings of the 1st ACM workshop on Mobile internet through cellular networks*. ACM, 2009, pp. 19–24.

[12] J. Rodríguez-Piñeiro, P. Suárez-Casal, J. García-Naya, L. Castedo, C. Briso-Rodríguez, and J. I. Alonso-Montes, "Experimental validation of ICI-aware OFDM receivers under time-varying conditions," in *IEEE Sensor Array and Multichannel Signal Processing Workshop*, 2014.

[13] S. Caban, J. Rodas, and J. A. García Naya, "A methodology for repeatable, off-line, closed-loop wireless communication system measurements at very high velocities of up to 560 km/h," in *Proc. 2011 IEEE International Instrumentation and Measurement Technology Conference (I2MTC2011)*, 2011.

[14] A. Molisch, *Wireless Communications*. Wiley, 2005.

[15] P. Robertson and S. Kaiser, "The effects of Doppler spreads in OFDM(A) mobile radio systems," in *IEEE 50th Vehicular Technology Conference VTC 1999 - Fall.*, 1999, pp. 329–333 vol.1.

[16] G. Taricco and E. Biglieri, "Space-time decoding with imperfect channel estimation," *IEEE Transactions on Wireless Communications*, vol. 4, no. 4, pp. 1874–1888, July 2005.

[17] S. Caban, J. Garcia Naya, and M. Rupp, "Measuring the physical layer performance of wireless communication systems: Part 33 in a series of tutorials on instrumentation and measurement," *IEEE Instrumentation Measurement Magazine*, vol. 14, no. 5, pp. 8–17, 2011.

[18] H. W. Lilliefors, "On the Kolmogorov-Smirnov test for normality with mean and variance unknown," *Journal of the American Statistical Association*, vol. 62, no. 318, pp. 399–402, 1967.